

Elastic moduli and strength of nanocrystalline cubic BC₂N from x-ray diffraction under nonhydrostatic compression

Haini Dong and Duanwei He*

Institute of Atomic and Molecular Physics, Sichuan University, Chengdu 610065, China

Thomas S. Duffy

Department of Geosciences, Princeton University, Princeton, New Jersey 08544, USA

Yusheng Zhao

LANSCE Division, Los Alamos National Laboratory, Los Alamos, New Mexico 87545, USA

(Received 21 October 2008; revised manuscript received 8 December 2008; published 9 January 2009)

The stress behavior of nanocrystalline cubic boron carbon nitride (*c*-BC₂N) was investigated using radial and axial x-ray diffractions in the diamond-anvil cell under nonhydrostatic compression up to ~100 GPa. The radial x-ray diffraction (RXRD) data yield a bulk modulus $K_0 = 276 \pm 20$ GPa with a fixed pressure derivative $K'_0 = 3.4$ at $\psi = 54.7^\circ$, which corresponds to the hydrostatic compression curve. The bulk modulus obtained from axial x-ray diffraction (AXRD) gives a value of 420 ± 11 GPa. A comparative study of the observed compression curves from radial and axial diffractions shows that the ruby-fluorescence pressure scale may reflect the maximum stress under nonhydrostatic compression. It was found that nanocrystalline *c*-BC₂N sample could support a maximum differential stress of ~38 GPa when it started to yield at ~66 GPa under uniaxial compression. Moreover, the aggregate elastic moduli of the nanocrystalline *c*-BC₂N have been determined from the RXRD data at high pressures.

DOI: [10.1103/PhysRevB.79.014105](https://doi.org/10.1103/PhysRevB.79.014105)

PACS number(s): 64.30.Ef, 62.20.D-, 61.05.cp

I. INTRODUCTION

Cubic B-C-N phases are reported to have hardness higher than cubic boron nitride (*c*BN), along with better chemical stability and ability to withstand oxidation at a higher temperature than diamond.¹ This significantly adds the attractiveness to cubic B-C-N phases as superhard materials for potential industrial applications.¹⁻¹⁰ Of these cubic B-C-N phases, *c*-BC₂N is of special interest due to its Vickers hardness as high as about 70 GPa (Ref. 11) which is much higher than *c*BN (45–50 GPa) and close to diamond (75–100 GPa). Despite several reports on the synthesis of *c*-BC₂N (Refs. 2, 4, 11, and 12) and many theoretical calculations,⁶⁻¹⁰ direct experimental measurements of elastic properties, strength, and plastic deformation behavior are limited. Conflicting reports on the bulk modulus have been reported by different authors.²⁻⁵ In 2001, Solozhenko *et al.*⁴ obtained a bulk modulus of 282 ± 15 GPa for *c*-BC₂N using traditional axial x-ray diffraction (AXRD) under quasihydrostatic compression to 30 GPa. Tkachev *et al.* used the same *c*-BC₂N samples as Ref. 4 to investigate the elastic moduli by Brillouin scattering.³ The bulk and shear moduli were determined to be 259 ± 22 and 238 ± 8 GPa, respectively. The values of the bulk modulus obtained by Refs. 3 and 4 are much smaller than other studies which yield values of ~350 GPa.^{2,5} This difference in the bulk modulus of *c*-BC₂N may be due to different experimental samples prepared from different synthesis conditions and different starting materials,⁸ as well as the effects of nonhydrostatic compression.

In this study, the compression curve and stress state of nanostructured *c*-BC₂N are examined systematically in the diamond-anvil cell (DAC) under nonhydrostatic conditions. Radial x-ray diffraction (RXRD) (Refs. 13–17) and associ-

ated lattice strain theory¹⁷⁻¹⁹ as well as the traditional AXRD were used in our experiments. In addition, a comparative study of the observed apparent compression curves from AXRD and RXRD data shows that the ruby-fluorescence pressure scale may reflect the maximum stress under nonhydrostatic compression. This means that the mean pressure obtained from the ruby-fluorescence scale is overestimated when the sample is subjected to nonhydrostatic compression. This is contrary to the previous report from Eggert *et al.*²⁰ that the nonhydrostatic ruby scale yielded lower pressures than hydrostatic pressure scale. Thus, there is a need for further exploration regarding the ruby-fluorescence pressure scale under nonhydrostatic compression.

II. EXPERIMENTS

The nanocrystalline *c*-BC₂N sample used in our experiments was synthesized in a two-stage multianvil press at 20 GPa and 1900°C from a ball-milled amorphous mixture of the hexagonal boron nitride (*h*BN) and graphite.¹¹ The ultrafine *c*-BC₂N nanocrystals (5–8 nm determined by high-resolution transmission electron microscopy) have a zinc-blende structure (ZnS) (fcc) with a cubic lattice parameter of 3.595 (7) Å. The nanostructured *c*-BC₂N sample was loaded into a 100- μ m-diameter sample hole in an amorphous Pd₄₀Ni₄₀P₄₀ gasket²¹ as well as a 90- μ m hole in a Be gasket for AXRD and RXRD measurements, respectively. The gaskets were preindented to ~25 μ m thickness at ~20 GPa. In AXRD experiment, one small chip of ruby (~5 μ m) was put on top within 10 μ m of the sample center for determining the pressures,²² another one was put on the amorphous Pd₄₀Ni₄₀P₄₀ gasket for pressure gradient measurement. A ~10 μ m Au foil was also put on top within 5 μ m of the

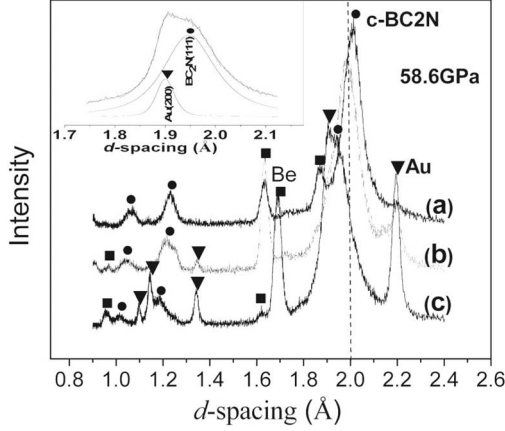


FIG. 1. RXRD Patterns of the sample taken at $\psi=0^\circ$ [curve (c)], 54.7° [curve (b)], and 90° [curve (a)] under the same loading. The position of BC_2N (111) peak at $\psi=54.7^\circ$ is marked by a dash line for comparison. BC_2N (111) peaks are overlapped by Au (200) peaks at $\psi=0^\circ$ (on the top left). The locations of $c\text{-BC}_2\text{N}$, Au, and Be are marked by solid circles, triangles, and squares, respectively.

sample center served as pressure standard²³ as well as position reference for RXRD measurement. No pressure transmitting medium was used in either experiment. Energy-dispersive axial and radial x-ray diffraction^{13–17} experiments were performed in the diamond anvil cell at the X17C beam line of the National Synchrotron Light Source at Brookhaven National Laboratory. The diffracted intensity was detected by a solid-state Ge detector with a fixed Bragg angle at $2\theta=12.004(5)^\circ$. As many as 17 pressure steps were investigated in the AXRD experiment and ten for RXRD measurement. Except for the first step, RXRD patterns were taken at $\psi=0^\circ$, 54.7° , and 90° (ψ is the angle between DAC loading axis and diffraction plane normal), respectively. The stage was always rotated back to $\psi=0^\circ$ and data collected again to compare it with the beginning patterns in the RXRD experiment.

III. THEORY

The sample in a gasketed diamond-anvil cell is subjected to a macroscopic differential stress t due to the uniaxial stress field under nonhydrostatic compression. In addition, a microscopic deviatoric stress ν also exists under nonhydrostatic compression and this is caused by heterogeneous deviatoric strain at each grain of the polycrystalline sample. The macroscopic differential stress can be given by $t=6G\langle Q(hkl)\rangle$ under isostress condition.^{17–19} $\langle Q(hkl)\rangle$ presents the average $Q(hkl)$ value over all observed reflections [diffraction lines of (111), (220), and (311) for $c\text{-BC}_2\text{N}$], while G is the aggregate shear modulus of the polycrystalline sample. And the local deviatoric stress is determined by $\nu=\varepsilon E$,²⁴ where ε is the microscopic deviatoric strain distribution, and E is the aggregate Young's modulus of the sample. The two types of stress distributions in a polycrystalline sample under nonhydrostatic compression allow two primary approaches to determine the strength of materials presently by analyzing x-ray diffraction peak broadening^{24–28}

and peak shifts^{13–17} together with lattice strain theory.^{17–19} These two methods should give the same value equaling to the sample's yield strength once plastic deformation is initialized in the sample, i.e.,^{15,29}

$$\varepsilon E = 6G\langle Q(hkl)\rangle = Y. \quad (1)$$

This has been well demonstrated in Refs. 15 and 29. The aggregate Young's modulus (E), shear modulus (G), and bulk modulus (K) have the relationship $E=9KG/(3K+G)$. Together with Eq. (1) the shear modulus and Young's modulus can be calculated as below once the sample is plastically deformed,

$$G = 3(K\varepsilon\langle Q(hkl)\rangle^{-1})/2 - 3K, \quad (2)$$

$$E = 9K - 18K\langle Q(hkl)\rangle\varepsilon^{-1}. \quad (3)$$

K , ε , and $\langle Q(hkl)\rangle$ can be obtained directly from RXRD measurements.²⁹ The above method is applicable only if both uniaxial differential stress and local deviatoric stress reach their upper limits, i.e., both equal to the yield strength of the sample under uniaxial loading.

IV. RESULTS AND DISCUSSION

Figure 1 shows the RXRD patterns taken at $\psi=0^\circ$, 54.7° , and 90° at 58.6 GPa to present typical peak profile changes with angle ψ . The diffraction peaks shifted to smaller d spacing as the angle ψ decreased, which reflects the increase in elastic strain as the diffraction plane normal approaches to the maximum stress axis. From lattice strain theory,^{17–19} the observed d spacing at $\psi=54.7^\circ$ equals the hydrostatic d spacing of the sample. So the hydrostatic compression curve can be directly derived from the diffraction data at $\psi=54.7^\circ$. As shown in Fig. 1, the diffraction lines of $c\text{-BC}_2\text{N}$ (111), (220), and (311) are available for data analysis. The lattice parameters of Au were derived from the XRD peaks of (111), (200), (220), and (311).

The observed relative volume change (V/V_0) at each pressure step from RXRD at $\psi=90^\circ$ and AXRD are shown in Fig. 2. According to the diffraction geometry, AXRD experiment is approximately equivalent to the RXRD measurement performed at $\psi=90^\circ$.¹⁵ Thus the value of V/V_0 from RXRD at $\psi=90^\circ$ and AXRD both give the lattice strain in the minimum stress direction. Pressures at $\psi=90^\circ$ for the RXRD data are determined from mean lattice parameters of gold at $\psi=54.7^\circ$, which represents the mean pressure value at each load. But for AXRD compression cure, the pressures are determined by the ruby-fluorescence scale, which is derived from the relationship of ruby-fluorescence line (R_1) shifts with pressures determined from the equation of state (EOS) of Pd, etc.²² Although this pressure scale is widely used, whether the ruby-fluorescence scale reflects the corresponding mean pressures under nonhydrostatic conditions is unclear up to now as there is insufficient experimental data to confirm it. Interestingly, we found that the compression cure from RXRD at $\psi=90^\circ$ (circles) of which pressure is determined at $\psi=54.7^\circ$ lies below that from AXRD (triangles) data (Fig. 2). As the sample environment and DAC

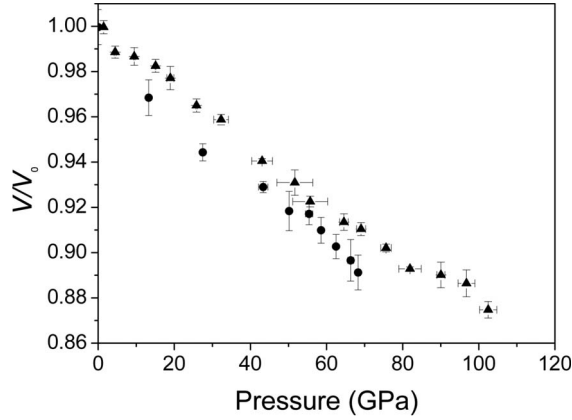


FIG. 2. Observed apparent V/V_0 of BC_2N from RXRD measurements at $\psi=90^\circ$ (solid circles) and AXRD (triangles) under different pressures. The pressures at $\psi=90^\circ$ for RXRD data are determined from the mean lattice parameter of gold at $\psi=54.7^\circ$ and the pressure for AXRD is determined by ruby-fluorescence pressure scale.

geometry are similar, we can assume that the stress distribution is about the same for c - BC_2N both in the AXRD and RXRD experiments. The above results indicate that the mean pressures calibrated by ruby-fluorescence scale under nonhydrostatic condition are overestimated. As far as we know, the pressure achieved in the maximum stress direction is the largest under uniaxial loading. Therefore, we suspect that the ruby-fluorescence pressure scale may reflect a maximum stress state under nonhydrostatic compression. Then the commonly used ruby-fluorescence pressure scale may cause large error for nonhydrostatic experiments, especially if the samples are strong materials. The stronger materials are the larger differential stress they can sustain under axial loading. This will lead to a larger difference between the maximum and minimum stress for stronger materials under high uniaxial compression.

The P - V data from the RXRD measurements at $\psi=0^\circ$, 54.7° , and 90° and the AXRD experiment are fitted to the third-order Birch-Murnaghan equation of state (Fig. 3) which yield the apparent bulk modulus (K_0) of each compression curve with the pressure derivative ($K'_0=dK_T/dP$ at $P=0$ GPa, where K_T is the isothermal bulk modulus) fixed at 3.4. The choice of K'_0 is based on the fact that the pressure derivative for diamond is 3.0 (1) (Ref. 30) and for c -BN is 4.0 ± 0.2 ,³¹ while the hardness of c - BC_2N (~ 70 GPa) is closer to that of diamond (75–100 GPa). Additionally, the choice of $K'_0=3.4$ gives a comparatively better fit for the compression curve data. The fitted results for the apparent bulk modulus are 184 ± 17 (RXRD at $\psi=0^\circ$), 276 ± 20 (RXRD at $\psi=54.7^\circ$), 350 ± 17 (RXRD at $\psi=90^\circ$), and 420 ± 11 GPa (AXRD), respectively. It can be seen that for a superhard material, such as c - BC_2N , diffraction orientation relative to the stress axis can have large effects on the bulk modulus determination from the nonhydrostatic compression experiment. Table I shows a comparison of the bulk modulus of diamond, c -BN, and c - BC_2N obtained from the published work and from our experiments. The bulk modulus $K_0=276 \pm 20$ GPa at $\psi=54.7^\circ$ for c - BC_2N is in general con-

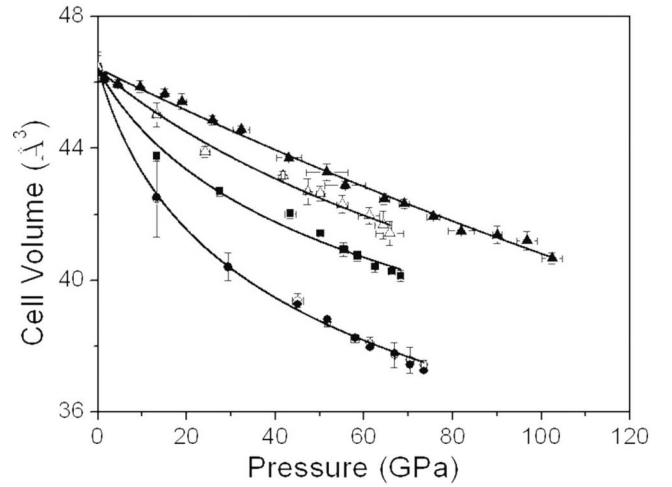


FIG. 3. Compression curves of c - BC_2N from lattice parameters measured by AXRD (solid triangles) and RXRD at $\psi=0^\circ$ (circles), 54.7° (squares), and 90° (open triangles). The pressures for RXRD data points are calculated from the measured diffraction data of gold at $\psi=0^\circ$, 54.7° , and 90° , respectively. Ruby-fluorescence scale is used for pressure determination in the AXRD data process. Open and solid circles at $\psi=0^\circ$ correspond to measurements at the beginning and end of the cycle for a given pressure step. The solid lines are third-order Birch-Murnaghan equation fit to the data.

sistent with that by Brillouin scattering from Ref. 3 as well as in accord with the value from x-ray diffraction under quasihydrostatic condition;⁴ while, it is much smaller than 350 GPa from x-ray diffraction measurements using a 4:1 methanol-ethanol pressure medium to maintain quasihydrostatic condition up to high pressures.^{2,5} However, a completely hydrostatic environment cannot be sustained above ~ 15 GPa due to the freezing of all known pressure media at ambient temperature.³² In fact, it is known that methanol-ethanol mixtures become highly nonhydrostatic above the freezing temperature. So the bulk modulus of 350 GPa for c - BC_2N from Knittle *et al.*³³ might be overestimated due to nonhydrostatic stresses caused by the strength of the pressure

TABLE I. A summary of the bulk modulus (K_0) of diamond, c -BN, and c - BC_2N , and their pressure derivative (K'_0) obtained from various methods, where (m) and (n) indicate microcrystalline and nanocrystalline starting materials, respectively.

Structure	K_0 (GPa)	K'_0	Reference
Diamond	446(1)	3.0(1)	30
c -BN	369 ± 14	4.0 ± 0.2	31
c - $BC_2N(n)$	276 ± 20	3.4 (fixed)	This study $\psi=54.7^\circ$
	184 ± 17	3.4 (fixed)	This study $\psi=0^\circ$
	350 ± 17	3.4 (fixed)	This study $\psi=90^\circ$
	420 ± 11	3.4 (fixed)	This study AXRD
c - $B_{0.3}(CN)_{0.7}(m)$	355 ± 19	4 (assumed)	2
c - $BC_2N(n)$	259 ± 22		3
c - $BC_2N(n)$	282 ± 15	4.3 ± 1.1	4
c - BC_2N	345		5

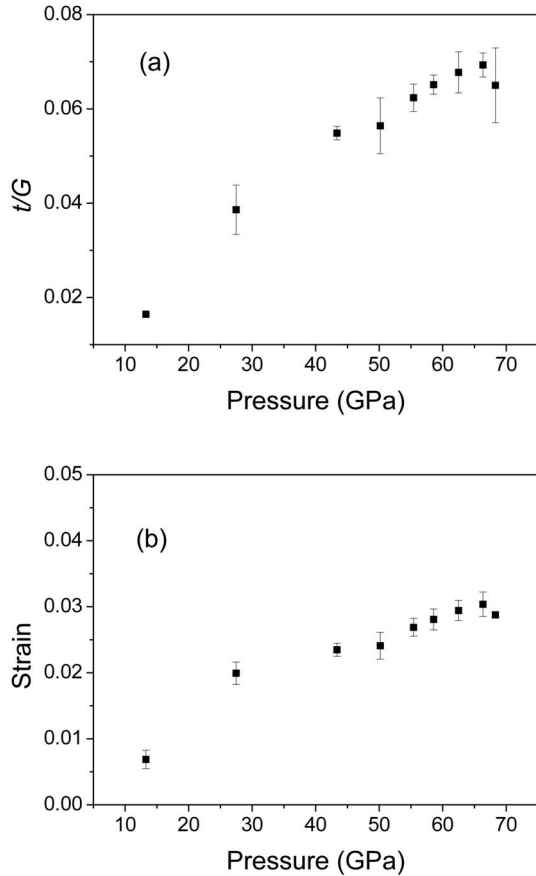


FIG. 4. (a) Ratio of differential stress to shear modulus (t/G) as a function of pressures for c -BC₂N. (b) Microscopic deviatoric strain distribution of c -BC₂N versus pressure. The pressure is determined from the mean lattice parameter of gold obtained at $\psi = 54.7^\circ$ from RXRD measurements.

media after freezing at high pressure. Also, this difference may be due to different grain size of different starting materials.³³ As discussed above, the mean pressure recorded by ruby-fluorescence in AXRD is likely overestimated, so the AXRD compression cure lies above that from RXRD at $\psi = 90^\circ$, even though both are measured close to the minimum stress direction. This leads to the bulk modulus determined from the RXRD measurements at $\psi = 90^\circ$ being much smaller than the value from AXRD. Also, it is interesting to note that the hydrostatic bulk modulus of c -BC₂N is smaller than that of c -BN although its hardness is higher than c -BN.¹¹ This implies that the bulk modulus is not a direct qualitative predictor of hardness for superhard materials. Moreover, the shear modulus of c -BC₂N is also smaller than c BN.⁴

The ratio of differential stress to shear modulus t/G for c -BC₂N was found to range from 0.02 to 0.07 at 13–69 GPa [Fig. 4(a)]. The value of t/G at each pressures step is obtained from the slop of the linear relationship between the observed d spacing and $1 - 3 \cos^2 \psi$.^{13–17} The ratio of t/G reaches the highest around 66 GPa and then levels off [Fig. 4(a)]. This corresponds with the trend of variation in microscopic deviatoric strain distribution ε (ε at each pressure step is derived from the linear plot of square of peak broadening

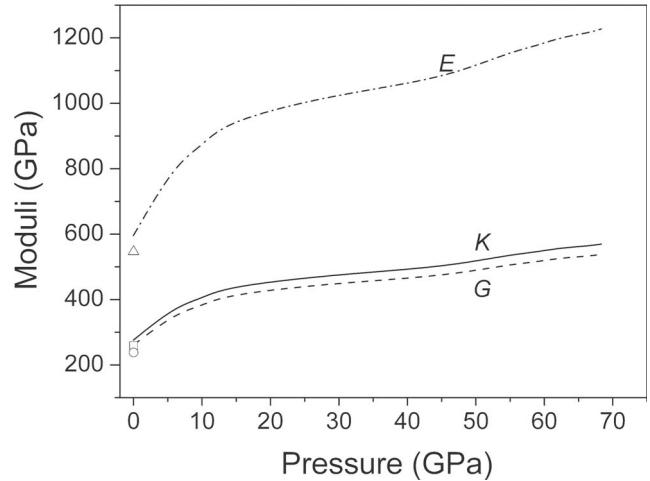


FIG. 5. Elastic moduli of c -BC₂N at different pressures. The K , G , and E are marked by solid, dash, and dash-dotted lines, respectively. The open circle, square, and triangle represent data at ambient condition from Brillouin scattering (Ref. 3).

versus the square of x-ray photon energy²⁴), which also reaches its highest value at $P=66$ GPa ($\varepsilon=0.03$) then levels off upon further compression [Fig. 4(b)]. These changes suggest that the macro/bulk yield point was reached near this pressure and local deviatoric stresses partially relaxed due to the plastic flow.³⁴ We assume that t has reached its limiting value at pressures of 66–68 GPa, i.e., c -BC₂N started to yield at ~ 66 GPa. Under these conditions, the shear modulus and Young's modulus can be calculated at $P=66$ –68 GPa from Eqs. (2) and (3) with the bulk modulus at high pressures obtained from the third-order Birch-Murnaghan equation of state. The shear and Young's moduli at other pressure steps are obtained by extrapolation from the relationship between E and G at $P=66$ –68 GPa. The elastic moduli of c -BC₂N as functions of pressure are plotted in Fig. 5. The values of elastic moduli at $P=0$ GPa (open symbols) are from Brillouin scattering measurement.³ With the shear modulus known, the differential stress can be derived at each pressure step from $t=6G\langle Q(hkl) \rangle$. For comparison, the differential stresses versus pressure determined from x-ray diffraction in a radial geometry for c -BC₂N, B₆O,¹⁵ and γ -Si₃N₄ (Ref. 35) are plotted in Fig. 6. These materials were all reported to be superhard materials. Obviously, the differential stress sustained by c -BC₂N is larger than B₆O and γ -Si₃N₄. At ~ 66 GPa, as high as ~ 38 GPa of the differential stress is supported by c -BC₂N. For comparison, B₆O supports a differential stress of 30 GPa at a confining pressure of 65 GPa (Ref. 15) and cubic silicon nitride (γ -Si₃N₄) reaches a maximum differential stress of 23 GPa at 68 GPa.³⁵ Aside from diamond, c -BC₂N is the strongest material studied under nonhydrostatic compression. Previously, a study documented that the strength of polycrystalline materials increased with decreasing grain size.³⁶ Hence grain-size effects on high-pressure strength should also be taken into account in comparing c -BC₂N (nanocrystalline), B₆O (microcrystalline), and γ -Si₃N₄ (nanocrystalline).

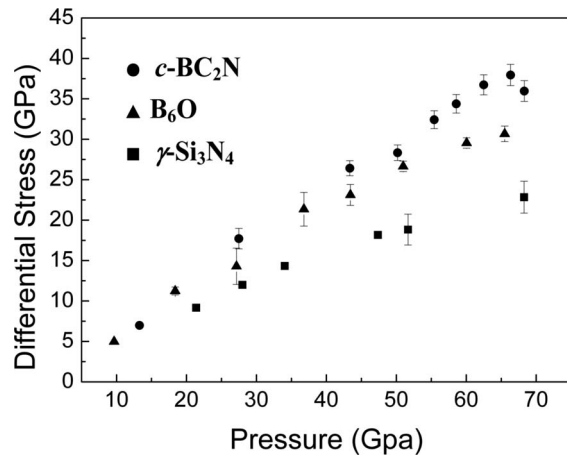


FIG. 6. A comparison of differential stress supported by $c\text{-BC}_2\text{N}$, $\gamma\text{-Si}_3\text{N}_4$, and B_6O under uniaxial compression.

V. CONCLUSION

In summary, the elastic and plastic properties of $c\text{-BC}_2\text{N}$ are systematically studied using AXRD and RXRD measurements. The EOS of $c\text{-BC}_2\text{N}$ corresponding to hydrostatic compression curve in RXRD at $\psi=54.7^\circ$ as well as nonhy-

drostatic compression curve from AXRD measurement are obtained. By analyzing the nonhydrostatic compression data, we determined the aggregate elastic moduli as functions of pressure. A differential stress of ~ 38 GPa at a confining pressure of ~ 66 GPa for $c\text{-BC}_2\text{N}$ was obtained. Furthermore, we found that ruby-fluorescence pressure scale may give a maximum stress state under nonhydrostatic compression through the comparative study of compression curves between AXRD and RXRD. Further studies are needed to confirm this.

ACKNOWLEDGMENTS

The authors thank J. Z. Hu, J. Shu, and H. K. Mao for experimental assistance. This work is partially supported by the Natural Science Foundation of China (Grants No. 50572067 and No. 10772126 to D.H.) and the Carnegie-DOE Alliance Center. This research was also partially supported by COMPRES, the Consortium for Materials Properties Research in Earth Sciences under NSF Cooperative Agreement No. EAR 06-49658. Use of the National Synchrotron Light Source, Brookhaven National Laboratory was supported by the U.S. Department of Energy, Office of Science, Office of Basic Energy Sciences under Contract No. DE-AC02-98CH10886.

*Author to whom correspondence should be addressed; duanweihe@yahoo.com

- ¹H. Sun, S. H. Jhi, D. Roundy, M. L. Cohen, and S. G. Louie, *Phys. Rev. B* **64**, 094108 (2001).
- ²E. Knittle, R. B. Kaner, R. Jeanloz, and M. L. Cohen, *Phys. Rev. B* **51**, 12149 (1995).
- ³S. N. Tkachev, V. L. Solozhenko, P. V. Zinin, M. H. Manghnani, and L. C. Ming, *Phys. Rev. B* **68**, 052104 (2003).
- ⁴V. L. Solozhenko, D. Andrault, G. Fiquet, M. Mezouar, and D. C. Rubie, *Appl. Phys. Lett.* **78**, 1385 (2001).
- ⁵W. Utsumi, S. Nakano, K. Kimoto, T. Okada, M. Isshiki, T. Taniguchi, K. Funakoshi, M. Akaishi, and O. Shimomura, *Proceedings of AIRAPT-18*, Beijing, China, 2001 (unpublished), p. 186.
- ⁶S. Chen, X. G. Gong, and S.-H. Wei, *Phys. Rev. Lett.* **98**, 015502 (2007).
- ⁷Z. C. Pan, H. Sun, and C. F. Chen, *Phys. Rev. Lett.* **98**, 135505 (2007).
- ⁸E. Kim, T. Pang, W. Utsumi, V. L. Solozhenko, and Y. Zhao, *Phys. Rev. B* **75**, 184115 (2007).
- ⁹S. Chen, X. G. Gong, and S.-H. Wei, *Phys. Rev. B* **77**, 014113 (2008).
- ¹⁰Y. Tateyama, T. Ogitsu, K. Kusakabe, S. Tsuneyuki, and S. Itoh, *Phys. Rev. B* **55**, R10161 (1997).
- ¹¹Y. Zhao, D. W. He, L. L. Daemen, T. D. Shen, R. B. Schwarz, Y. Zhu, D. L. Bish, J. Huang, J. Zhang, G. Shen, J. Qian, and T. W. Zerda, *J. Mater. Res.* **17**, 3139 (2002).
- ¹²T. Komatsu, M. Nomura, Y. Kakudate, and S. Fujiwara, *J. Mater. Chem.* **6**, 1799 (1996).
- ¹³S. R. Shieh, T. S. Duffy, and B. S. Li, *Phys. Rev. Lett.* **89**,

255507 (2002).

- ¹⁴T. S. Duffy, G. Shen, D. L. Heinz, J. Shu, Y. Ma, H. K. Mao, R. J. Hemley, and A. K. Singh, *Phys. Rev. B* **60**, 15063 (1999).
- ¹⁵D. He, S. R. Shieh, and T. S. Duffy, *Phys. Rev. B* **70**, 184121 (2004).
- ¹⁶T. S. Duffy, G. Shen, J. Shu, H. K. Mao, R. J. Hemley, and A. K. Singh, *J. Appl. Phys.* **86**, 6729 (1999).
- ¹⁷A. K. Singh, C. Balasingh, H. K. Mao, R. J. Hemley, and J. Shu, *J. Appl. Phys.* **83**, 7567 (1998).
- ¹⁸A. K. Singh, *J. Appl. Phys.* **73**, 4278 (1993).
- ¹⁹A. K. Singh, H. Mao, J. Shu, and R. J. Hemley, *Phys. Rev. Lett.* **80**, 2157 (1998).
- ²⁰J. H. Eggert, K. A. Goettel, and I. F. Silvera, *Phys. Rev. B* **40**, 5724 (1989).
- ²¹D. He, Y. Zhao, T. D. Sheng, R. B. Schwarz, J. Qian, K. A. Lokshin, S. Bobev, L. L. Daemen, H. K. Mao, J. Z. Hu, J. Shu, and J. Xu, *Rev. Sci. Instrum.* **74**, 3012 (2003).
- ²²H. K. Mao and P. M. Bell, *J. Appl. Phys.* **49**, 3276 (1978).
- ²³S.-H. Shim, T. S. Duffy, and T. Kenichi, *Earth Planet. Sci. Lett.* **203**, 729 (2002).
- ²⁴D. J. Weidner, Y. Wang, and M. T. Vaughan, *Science* **266**, 419 (1994).
- ²⁵D. J. Weidner, Y. Wang, and M. T. Vaughan, *Geophys. Res. Lett.* **21**, 753 (1994).
- ²⁶J. Chen, D. J. Weidner, and M. T. Vaughan, *Nature (London)* **419**, 824 (2002).
- ²⁷H. P. Klug and L. E. Alexander, *X-Ray Diffraction Procedures* (Wiley, New York, 1974).
- ²⁸B. Warren, *X-Ray Diffraction* (Addison-Wesley, London, 1989).
- ²⁹D. He and T. S. Duffy, *Phys. Rev. B* **73**, 134106 (2006).

- ³⁰F. Occelli, P. Loubeyre, and R. L. Toullec, *Nature Mater.* **2**, 151 (2003).
- ³¹E. Knittle, R. M. Wentzcovitch, R. Jeanloz, and M. L. Cohen, *Nature (London)* **337**, 349 (1989).
- ³²R. Miletich, D. R. Allan, and W. F. Kuhs, *Rev. Mineral. Geochem.* **41**, 447 (2000).
- ³³B. Chen, D. Penwell, L. R. Benedetti, R. Jeanloz, and M. B. Kruger, *Phys. Rev. B* **66**, 144101 (2002).
- ³⁴Y. Zhao, J. Zhang, B. Clausen, T. D. Shen, G. T. Gray III, and L. Wang, *Nano Lett.* **7**, 426 (2007).
- ³⁵B. Kiefer, S. R. Shieh, T. S. Duffy, and T. Sekine, *Phys. Rev. B* **72**, 014102 (2005).
- ³⁶A. K. Singh, H. P. Liermann, and S. K. Saxena, *Solid State Commun.* **132**, 795 (2004).